ADVANCED FUNCTIONAL MATERIALS

Supporting Information

for *Adv. Funct. Mater.*, DOI: 10.1002/adfm.201905971

Making Fiber-Shaped Ni//Bi Battery Simultaneously with High Energy Density, Power Density, and Safety

Mengying Wang, Songlin Xie, Chengqiang Tang, Yang Zhao, Meng Liao, Lei Ye, Bingjie Wang, and Huisheng Peng**

Supporting Information

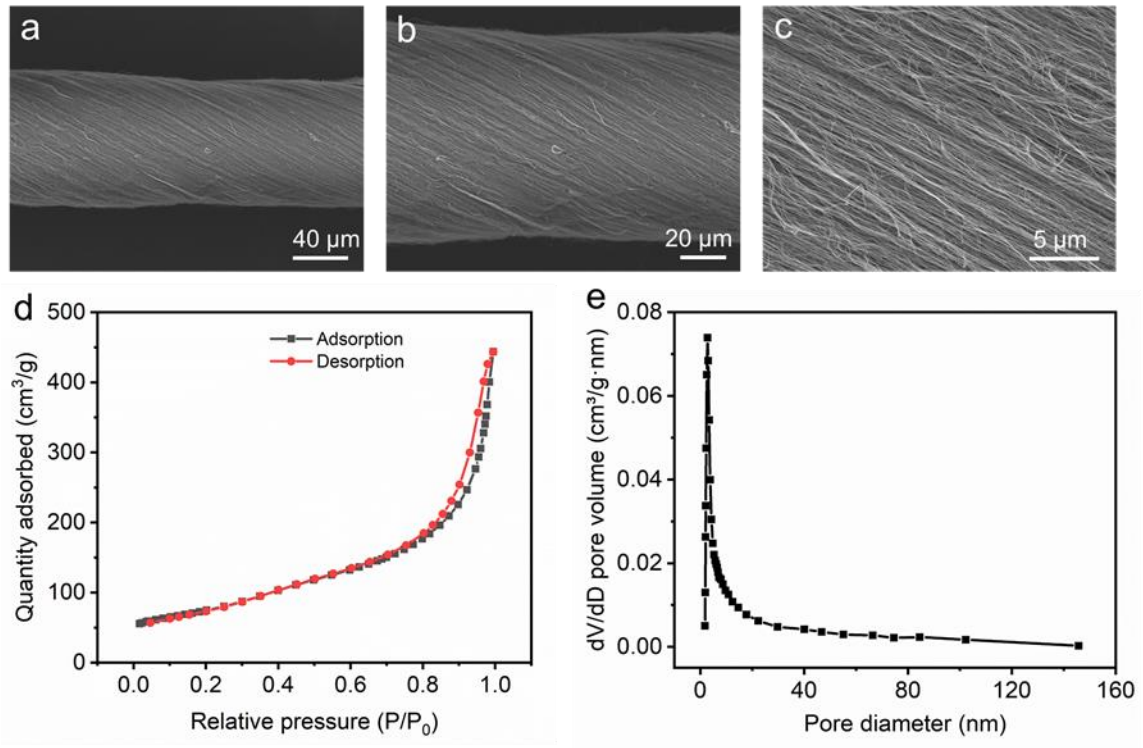

Figure S1. a-c) SEM images of CNT fiber at low and high magnifications. d, e) N_2 adsorption-desorption isotherms and the pore diameter of CNT fiber.

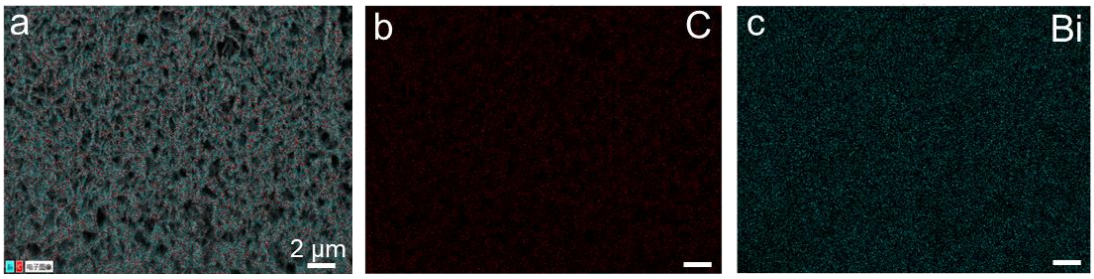

Figure S2. a-c) Energy dispersive spectroscopy (EDS) elemental mapping of the rGO/Bi hybrid.

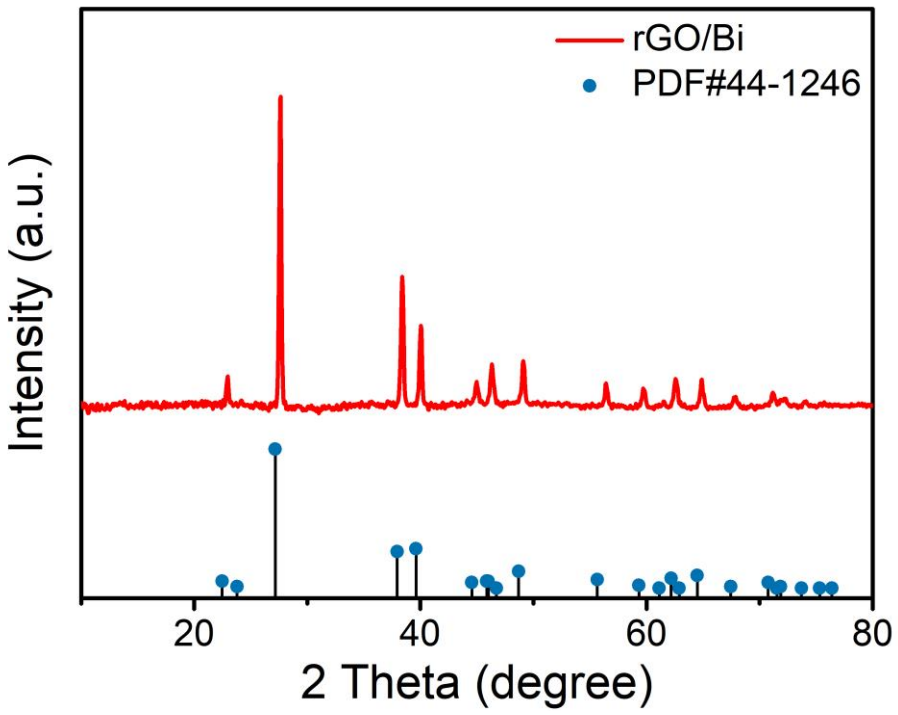

Figure S3. XRD patterns of the rGO/Bi hybrid and the reference.

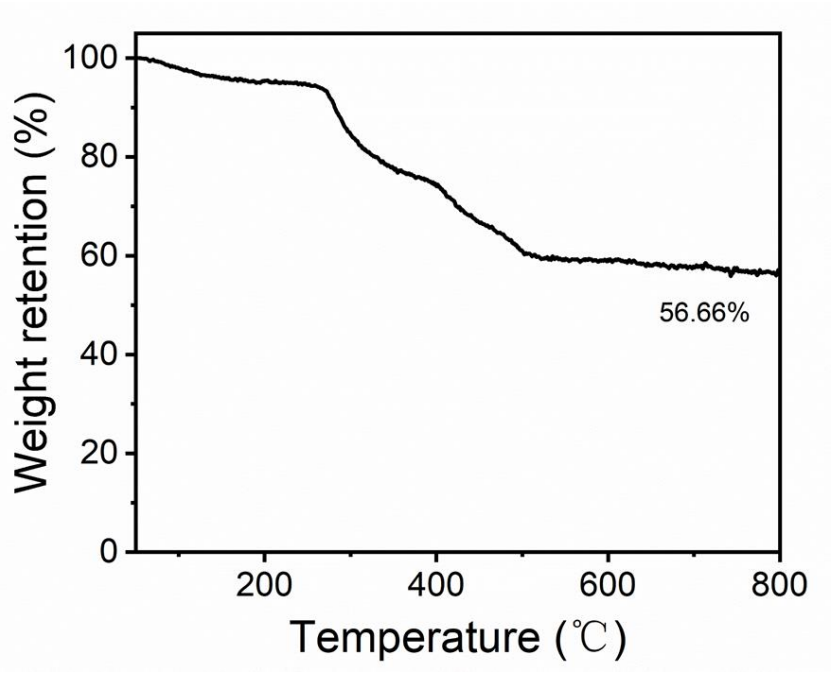

Figure S4. Thermogravimetric analysis (TGA) of the rGO/Bi/CNT fiber electrode.

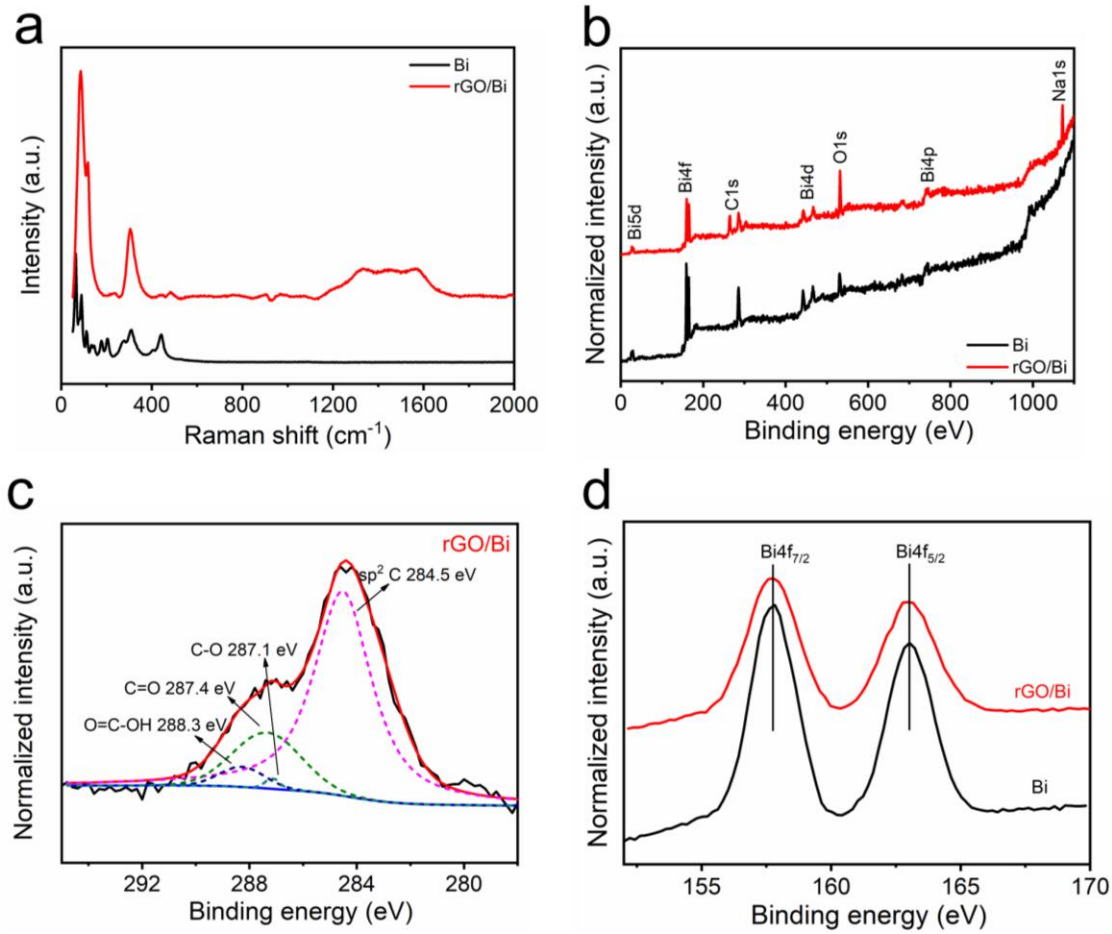

Figure S5. a-d) Raman spectra, full XPS spectra, C 2s XPS spectra and Bi 4f XPS spectra of the rGO/Bi hybrid, respectively.

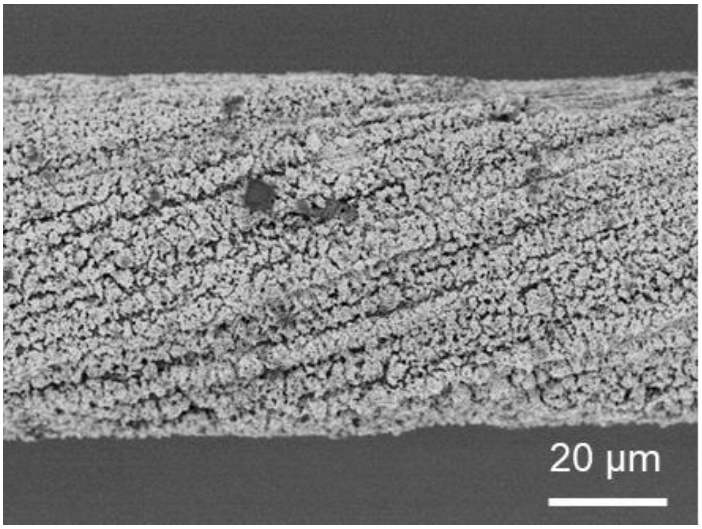

Figure S6. SEM image of a Bi/CNT fiber.

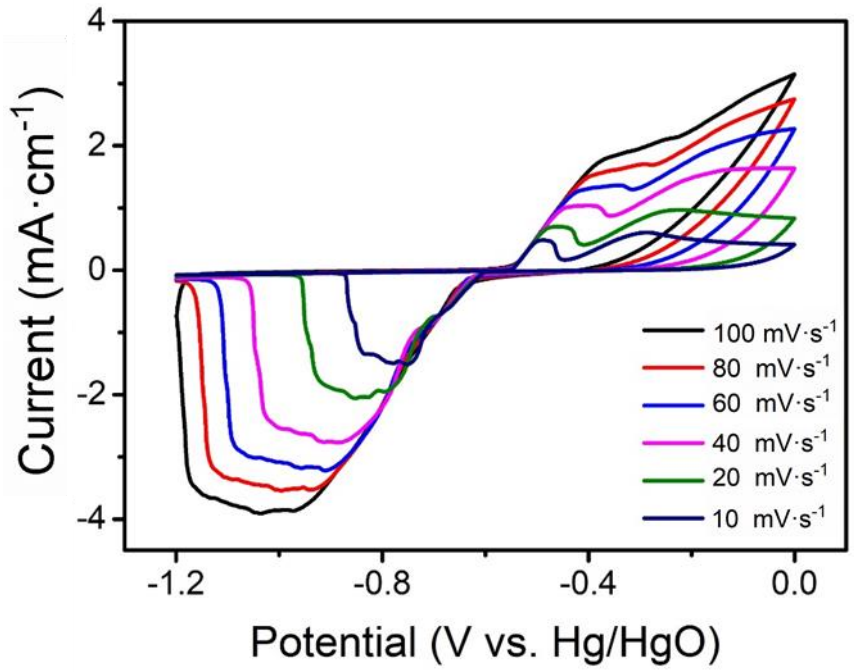

Figure S7. CV curves of the rGO/Bi/CNT fiber electrode at increasing scan rates.

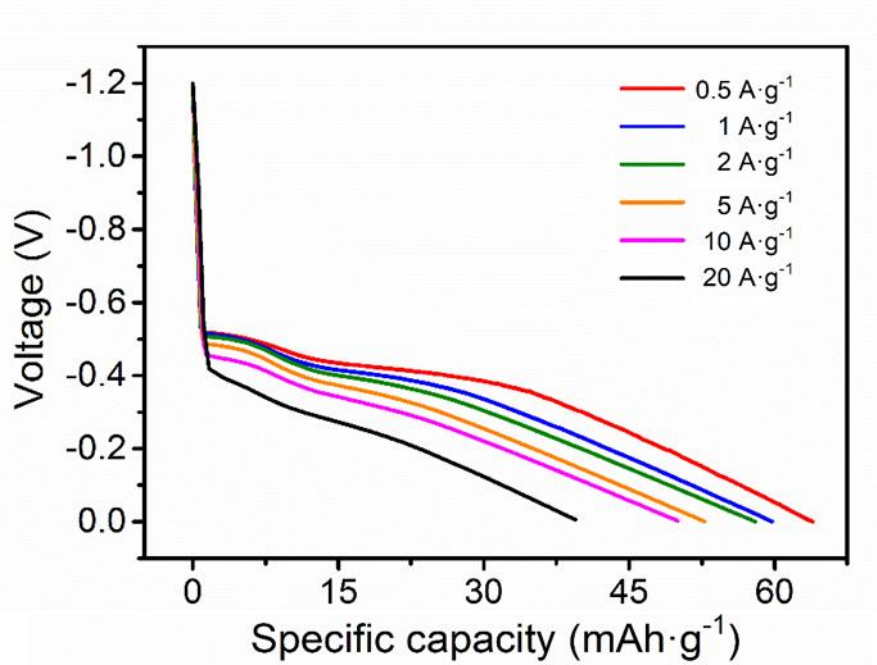

Figure S8. Galvanostatic discharge profiles of the Bi/CNT fiber electrode at increasing current densities.

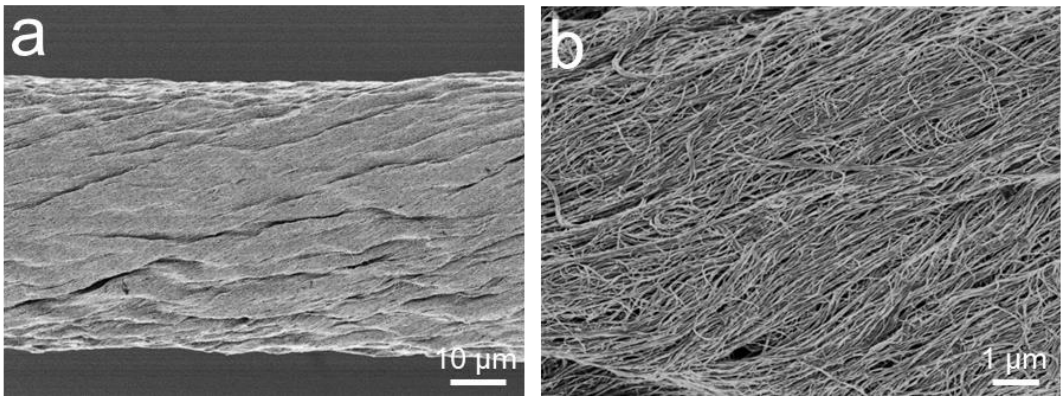

Figure S9. a, **b**) SEM images of Bi/CNT fiber electrode after 2000 cycles at low and high magnifications, respectively.

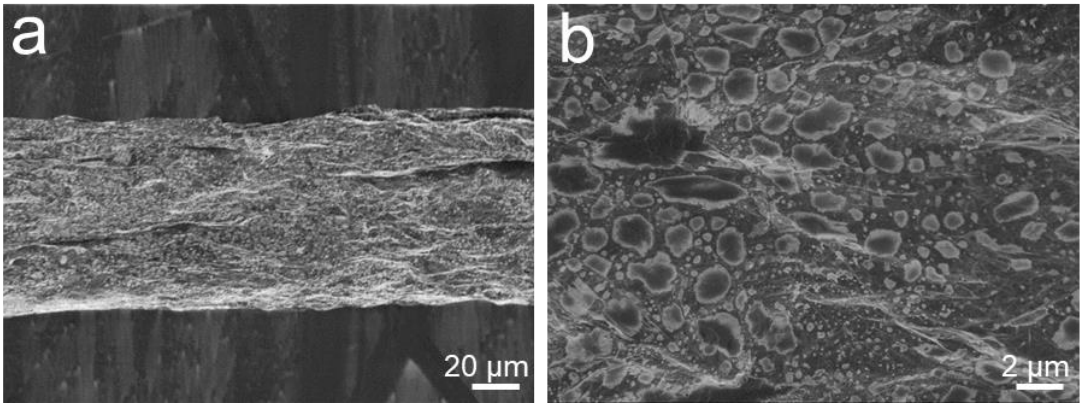

Figure S10. a, **b**) SEM images of rGO/Bi/CNT fiber electrode after 2000 cycles at low and high magnifications, respectively.

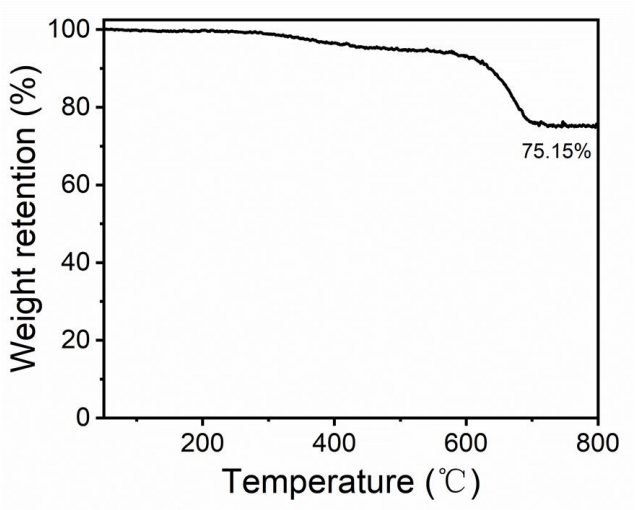

Figure S11. TGA curve of the rGO/Ni/NiO/CNT fiber electrode.

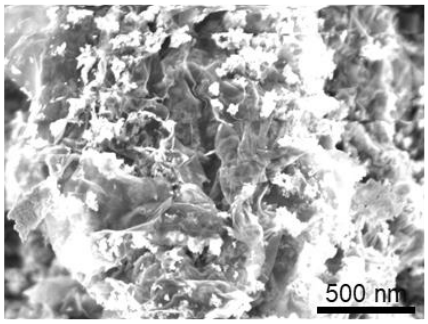

Figure S12. SEM image of rGO/NiO hybrid.

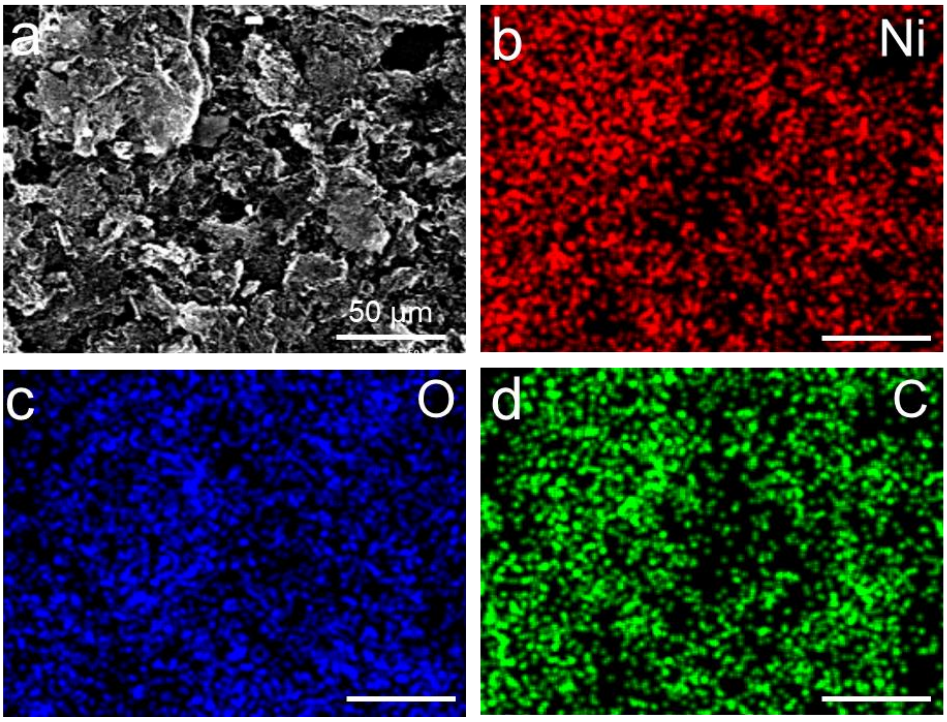

Figure S13. EDS elemental mapping of rGO/Ni/NiO hybrid.

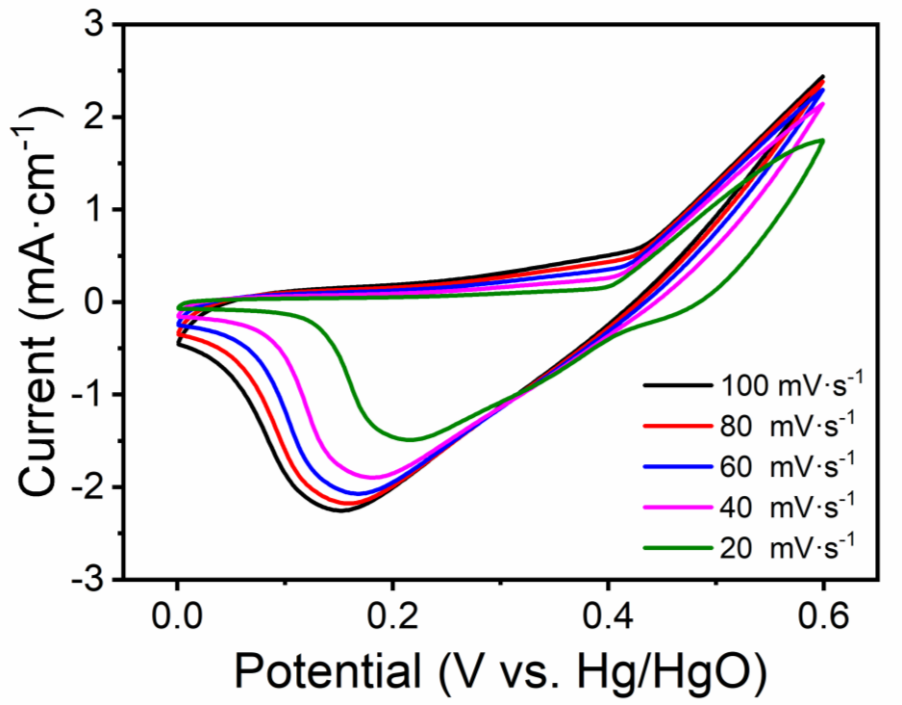

Figure S14. CV curves of the rGO/Ni/NiO/CNT fiber electrode.

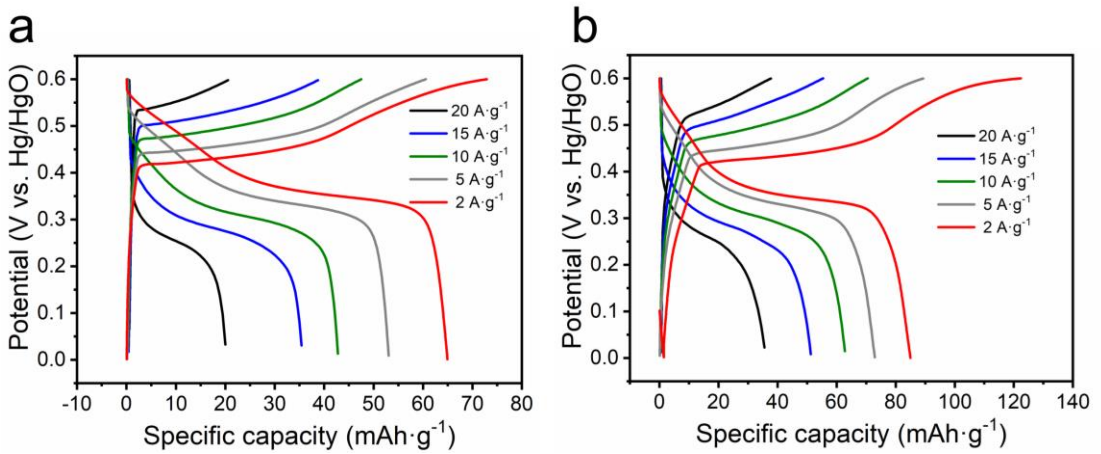

Figure S15. a, **b**) Galvanostatic charge and discharge profiles of the NiO/CNT and rGO/NiO/CNT fiber electrodes, respectively.

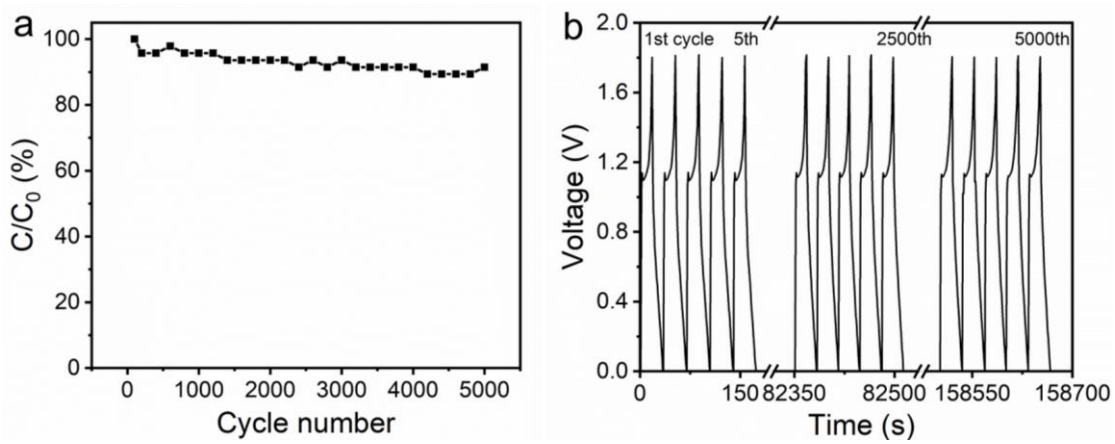

Figure S16. a) Cycling performance of fiber-shaped Ni//Bi battery at 20 $A \cdot g^{-1}$ for 5,000 cycles. b) Galvanostatic charge and discharge profiles after different cycle numbers.

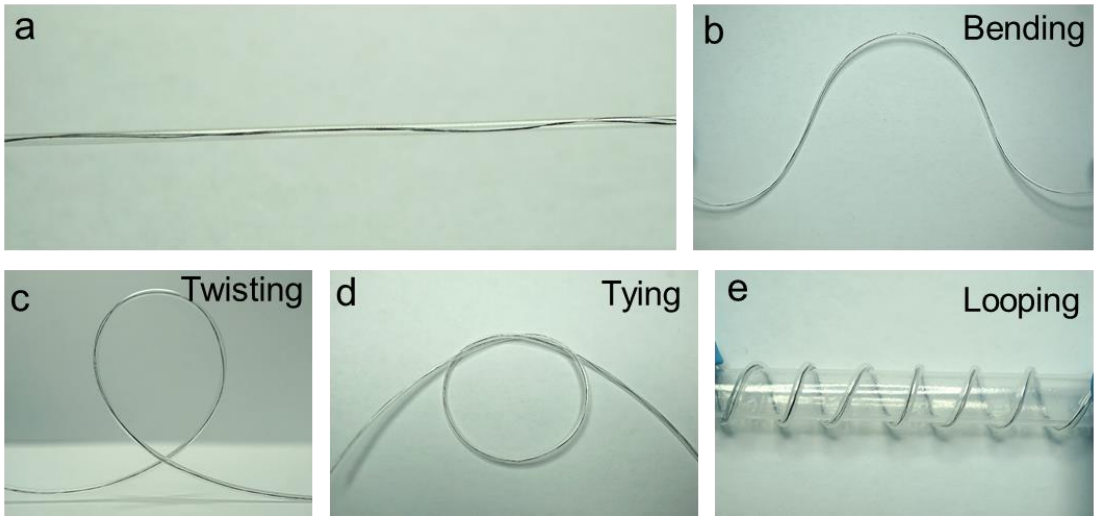

Figure S17. Photographs of the fiber-shaped Ni-Bi battery being deformed into different shapes.

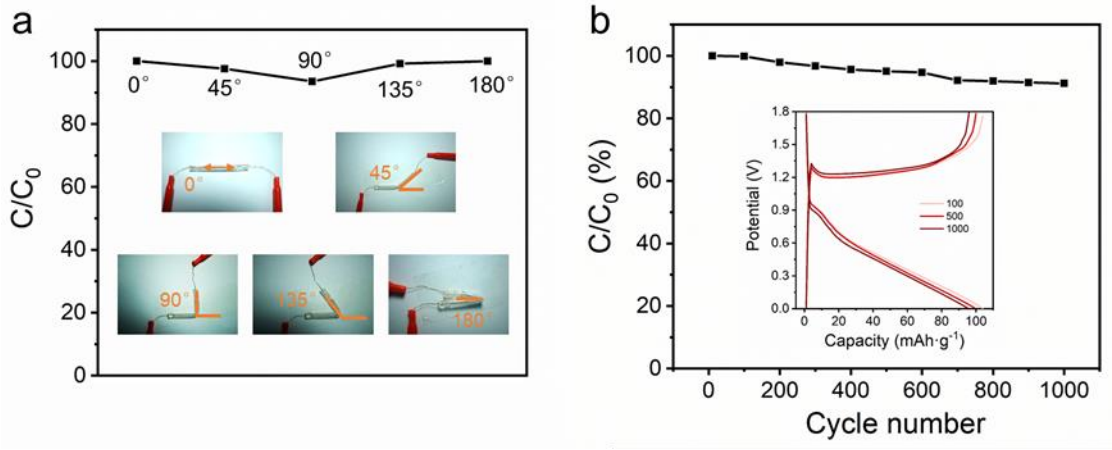

Figure S18. a) Capacity retention of the fiber-shaped Ni-Bi battery under different bending conditions. b) Capacity retention of the fiber-shaped Ni-Bi battery after bending for 1,000 cycles at the bending angle of 90° (inset, Galvanostatic charge and discharge profiles of the fiber-shaped Ni-Bi battery).

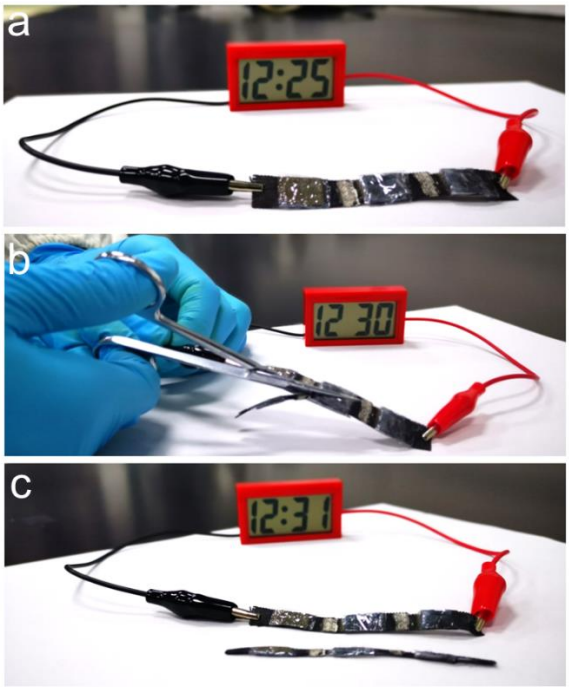

Figure S19. Photographs of three Ni//Bi battery textiles connected in series to power a commercial electronic watch before (**a**), under (**b**) and after (**c**) cutting.